



# Managing the Risk of Wellbore Instability Using Geomechanical Modeling and Wellbore Stability Analysis for Muzhil Shale Formation in Gulf of Suez, Egypt

Received 24 March 2023; Revised 15 June 2023; Accepted 16 June 2023

Ahmed S. Mohamed<sup>1</sup>  
Awad A. Omran<sup>2</sup>  
Mustafa T. Mohamed<sup>3</sup>  
Bassem S. Nabawy<sup>4</sup>

## Keywords

Rock failure criteria,  
Wellbore instability  
Muzhil field, Geomechanical  
model, well trajectory

## Abstract

Wellbore instability constitutes potential risks during wellbore drilling operation; these risks may cause complicated states, and in some cases, can lead to costly operational issues. In this study we present the best solution by predicting and quantifying wellbore instability in Muzhil field, Gulf of Suez, using a 1-DMechanical Earth Model (1DMEM) built with well logs, pressure measurements, and drilling events reports. Firstly, we created 1DMEM by calculating the pore pressure, vertical stress, rock strength, rock elastic parameters, and horizontal stresses. Mohr Coulomb, Modified Lade and Mogi Coulomb failure criteria determined the well deformation possibility. Lastly 1-DMEM can be used to conduct a comprehensive geo-mechanical wellbore stability analysis for the trouble zones of Muzhil Formation. 1-DMEM results showed that the best azimuth for Vertical and slightly inclined Wells will be (40°–60°) clockwise from the North, i.e., parallel to SHmin (NE40SW). The wellbore stability analysis showed that the vertical and low deviated wellbore (less than 40°) is safe and more stable than the horizontal and high deviated wellbore and unsuitable Mud Weight (MW) is a major cause of the wellbore instability. The optimal solution to wellbore instability is to follow the optimum wellbore path and use safe MW. The optimum MW in shale formation ranges from (13.5-15) ppg. The results contribute to the development plan of the wellbores nearby the studied area and reducing nonproductive time and cost.

## 1. Introduction

Wellbore instability is one of the major causes for wellbore failure and leads to several issues for drilling and completion operations. Several issues, such as stuck pipes, collapse, wellbore washouts, blowouts, breakout, kicks, and mud losses may take place due to a reduction of

<sup>1</sup> [Ahmedsayed8686@yahoo.com](mailto:Ahmedsayed8686@yahoo.com) Associate research, Dept. of Mining and Petroleum, Eng., Qena, Al-Azhar University

<sup>2</sup> [a3omran@aun.edu.eg](mailto:a3omran@aun.edu.eg) - professor, Dept. of Geology. Science, Assiut University

<sup>3</sup> [mostafa.amin@au.edu.eg](mailto:mostafa.amin@au.edu.eg) - professor, Dept. of Mining and Metallurgical. Eng., Assiut University

<sup>4</sup> [bsnabawy@yahoo.co.uk](mailto:bsnabawy@yahoo.co.uk) professor Dep. of Geophysical Sciences, National Research Centre, Cairo

accurate wellbore stability (WBS) analysis. Wellbore instability also increases the drilling costs and time, and sometimes leads to borehole abandonment before it attains its aim point. The costs on these issues is approximately 10% of the overall time of drilling on average [1]. Also, wellbore instability is a highly sophisticated problem and several factors such as rock mechanical parameters, wellbore trajectory, pore pressure (Pp), far-field principal stresses, drilling mud and pore fluid chemicals, mud density, time, and temperature are considered main factors [2]. Throughout the previous eras, numerous efforts have been attempted to improve WBS, and several numerical models and analytical approaches have been executed for analyzing WBS [3-8]. However, it still remains a major challenge for the industry of drilling, and about 1/3 of the nonproductive time (NPT) while drilling operations is due to wellbore issues, which mostly exist in shale formations [9]. In previous studies, the planned models for WBS are time-independent and the effects of all chemical, thermal, and poro-elastic factors are not simultaneously considered when estimating the wellbore shear failure gradient or the fracture gradient [10-25]. Muzhil oil is located in the offshore central part of the Gulf of Suez (G.O.S) between longitudes: 33° 7' 24" E and 33° 8' 24" E and latitudes: 28° 53' 12" N and 28° 54' 47" N. Muzhil field is sited between the Ras Budran and October oilfields. The concession occupies an area of almost 180 km<sup>2</sup> (Fig. 1). Hydrocarbon was discovered in cretaceous and Miocene successions with oil and gas trapped in Matulla (Cretaceous) and Nukhel (Miocene) formations [26]. Comprehensive data set from 4 wells (Muzhil-1, Muzhil-2, Muzhil-4, and Muzhil-7) table (1) are used for evaluating and managing wellbore instability, to optimize MW, and reduce risks of wellbore instability using an integrated WBS analysis. So, the current study aims at reducing NPT and expenditure. The used data are licensed from Egyptian General Petroleum Corporation (EGPC) and obtained from South Abu Zienima Company (SAZ).

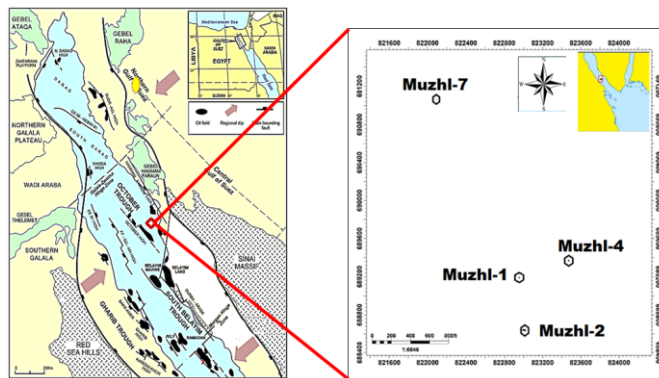


Fig. 1: Location map of the G.O.S, Abu Zienima concession and the studied wells in Muzhil field area.

## 2. Methods and tools

Datasets of deviated wellbore are analysed for forecasting the majority of wellbore instability issues that occurred in shaly formations. These data of this study are summarized in Table 1. The technique of identifying and decreasing the wellbore instability issues comprises the development of a geo-mechanical model using Techlog Software (Version 2015) [22].

### 2.1. Calculation of rock mechanical properties

#### 2.1.1 Dynamic elastic properties (isotropic properties)

The dynamic elastic parameters (such as Young's modulus (E), Poisson's ratio ( $\nu$ )) shear modulus, and bulk modulus) were estimated using the concept of elastic modulus equations

defined by Clark (1966) [20] from compressional acoustic wave velocity ( $v_p$ ) and shear acoustic wave velocity ( $v_s$ ) associated with the bulk density ( $\rho$ ) logs as in Equations. (1-4) [21] Fig. 2.

**Table 1: Summary of data used in this work.**

| Data                 | Muzhil-1 | Muzhil-2 | Muzhil-4 | Muzhil-7 |
|----------------------|----------|----------|----------|----------|
| DTCO- RHOB- GR       | ✓        | ✓        | ✓        | ✓        |
| DTSM                 | x        | ✓        | x        | ✓        |
| Well logs            | ✓        | ✓        | ✓        | ✓        |
| Borehole images      | x        | ✓        | ✓        | ✓        |
| Pressure measurement | ✓        | ✓        | ✓        | ✓        |
| Well report-FIT      | ✓        | ✓        | ✓        | ✓        |
| Drilling events      | ✓        | ✓        | ✓        | ✓        |

$$E_{\text{Dynamic}} = \rho v_s^2 \left( \frac{3v_p^3 - 4v_s^2}{v_p^2 - v_s^2} \right) \quad (1)$$

$$V_{\text{Dynamic}} = \frac{v_p^2 - v_s^2}{2(v_p^2 - v_s^2)} \quad (2)$$

$$G_{\text{dyn}} = (13474.45) \frac{\rho_b}{(\Delta t_{\text{shear}})^2} \quad (3)$$

$$K_{\text{dyn}} = (13474.45) \left[ \frac{\rho_b}{(\Delta t_{\text{comp}})^2} \right] - \frac{4}{3} G_{\text{dyn}} \quad (4)$$

## 2.1.2 Static properties (Dynamic to static formulas)

### 2.1.2.1 Static Young's modulus ( $E_{\text{static}}$ ) and Static Poisson Ratio ( $v_{\text{static}}$ ) Formula

The elastic values are generally obtained in the dynamic state, so dynamic values should be converted to static values by correlations [22-26] formula used to estimate  $E_{\text{static}}$  from  $E_{\text{dynamic}}$  (Equ.5). Many experimental studies showed that there is no major difference in values between the  $v_{\text{static}}$  and  $v_{\text{dynamic}}$  [22-25]. Thus, most literatures basically assumed that the  $v_{\text{dynamic}}$  almost equals to the  $v_{\text{static}}$  [28-29] Fig. 3.

$$E_{\text{static}} = 0.74(E_{\text{dynamic}}) - 0.82 \quad (5)$$

### 2.1.2 The Rock strength calculation

The rock strength procedure calculates the rock strength parameters to build the rock strength criteria in the earth geological module, and these parameters can be classified as follows.

#### 2.1.2.1 Uniaxial Compressive Strength (UCS) and Tensile Strength (TSTR)

There are numerous published empirical formulas for calculating the UCS from borehole logs, but every relation should be confirmed for a certain rock type [22, 27]. In this study, Dick plump formula was applied to estimate the UCS because it gives the best correlation in this field (Equ. 6). The tensile strength (TSTR) is calculated from TSTR directly from UCS [22-25] for this model, using the simple correlation (Equ. 7) to compute Fig. 4.

$$\text{UCS} = 4.242 \times 10^{-3} \times E_{\text{static}} \quad (6)$$

$$\text{TSTR} = 0.1 \times \text{UCS} \quad (7)$$

### 2.1.2.2 Internal Friction Angle ((FANG ( $\phi$ ))

The suitable approach to obtain the FANG  $\phi$  value is when a UCS test is carried out. In a case no core measurements are available, but  $\phi$  was estimated from available empirical equations. In the present case study, the Lal's formula (Equ. 8) for estimating the  $\phi$  from compressive sonic (DTCO) gives the best formula [32] (Fig. 4). Cohesion (CO) was estimated using UCS and  $\phi$  based on the following the theoretical correlation (Equ. 9):

$$\phi = \sin^{-1} \left( \left( \frac{304878}{Dt} - 1000 \right) / \left( \frac{304878}{Dt} + 1000 \right) \right) \quad (8)$$

$$C = \frac{UCS}{2 \left[ \sqrt{1 + (1 + \tan \phi)^2} + \tan \phi \right]} \quad (9)$$

## 2.2 Determination of in situ stresses magnitudes and orientation

### 2.2.1 Overburden Stress ( $S_v$ ) Estimation

$S_v$  was estimated using the Amoco method (Equ.10), which has been successfully applied in the Muzhil oilfield and many other basins globally [33], Fig.5.

$$\sigma_v = \int_0^z \rho b(z) g dz \quad (10)$$

Where ( $\rho b$ ) is the bulk density, ( $z$ ) is the true vertical depth, ( $g$ ) is gravitational acceleration.

### Pore pressure (Pp)

Eaton's correlation is commonly used to predict the formation Pp based on the sonic logs [34-35]. This correlation is formulated as shown in Equ.11 and Fig. 6, then the estimated Pp is calibrated using points of pressure recorded from the MDT.

$$P_p = s_v - (s_v - P_o) \left( \frac{Dt_o}{Dt_n} \right)^n \quad (11)$$

Where (Pp) is the Estimated Pore Pressure. ( $S_v$ ) is the vertical stress gradient. ( $P_o$ ) is the observed pressure gradient, ( $Dt_n$ ) is the normal compaction trend. ( $Dt_o$ ) is the observed transit time an ( $n$ ) is Eaton exponent parameter, ( $n$ ) =3.

### 2.2.2 Horizontal stresses ( $S_H, S_h$ )

#### 2.2.2.1. Orientation of horizontal stresses ( $S_H, S_h$ )

There are many tools to determine the horizontal stresses orientation; [33] The wellbore imaging represents the most powerful tool in identifying the breakout and the breakdown and consequently the azimuth of the  $S_H$  and  $S_h$  can be detected respectively. In this study, we used the data from FMI log of well Muzhil-4, which is analyzed and compared to the data from earthquake focal mechanism. We found that the azimuth of  $S_H$  is  $130^\circ$ .

#### 2.2.2.2 The maximum and minimum horizontal stress ( $S_H, S_h$ ) magnitudes

Poroelastic Horizontal Strain Model is generally the most used approach for horizontal stresses estimation. Assuming flat-layered poro-elasticity deformation in the formation, a pair of particular constant strains,  $\epsilon_h$  and  $\epsilon_H$  are applied to the formation in the directions of  $S_h$  and  $S_H$  respectively. The Poroelastic Horizontal Strain Model can be expressed using Estatic,  $\nu$ , Biot's constant,  $S_v$ , and Pp Eqs. (12-13). The  $\epsilon_h$  and  $\epsilon_H$  are not directly measured, and usually

measured by adjusting the strains, and can calibrate the estimated stresses with the measured horizontal stresses at depth [36].

$$\sigma_h = \frac{\nu}{1-\nu} \sigma_v - \frac{\nu}{1-\nu} \alpha P_p + \alpha P_p + \frac{\nu}{1-\nu^2} \epsilon_h + \frac{\nu E}{1-\nu^2} \epsilon_H \tag{12}$$

$$\sigma_H = \frac{\nu}{1-\nu} \sigma_v - \frac{\nu}{1-\nu} \alpha P_p + \alpha P_p + \frac{\nu}{1-\nu^2} \epsilon_H + \frac{\nu E}{1-\nu^2} \epsilon_h \tag{13}$$

Fig. 7 presents the estimated magnitudes of horizontal stresses. We notice the equalization between maximum and minimum horizontal stress magnitudes that tend to method the vertical stress magnitude in south Gharib and Baba formation. This is interrelated to the presence of the salt which behaves as visco-plastic material. Moreover, the estimated magnitude of the horizontal stresses, matches the normal stress regime in the G.O.S. area ( $S_V > S_{HMax} > S_{Hmin}$ ).

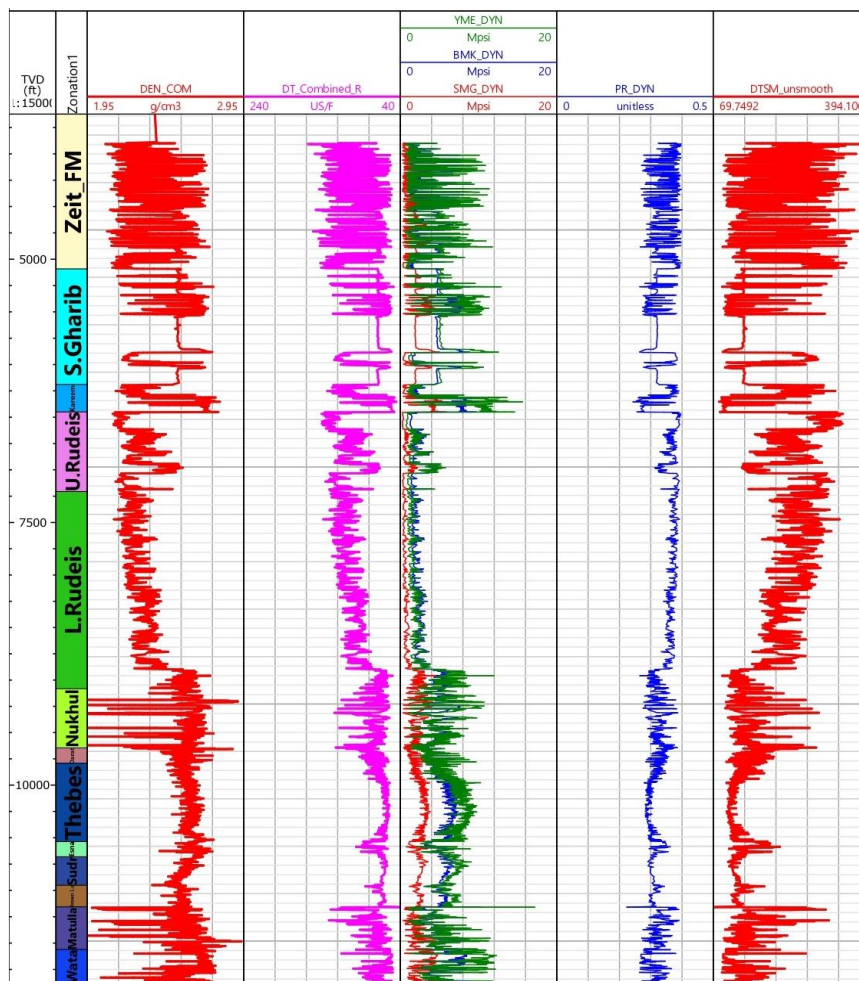


Fig. 2: Calculated dynamic elastic moduli of muzhil-7 wellbore.

**Track-1**(Depth), **track-2** (Zonation), **track-3**(density-com), **track-4**(Dt combiner), **track-5**(YM-DYN, BM-DYN, SM-DYN), **track-6**((PR-DYN), and **track-7**(shear sonic DT)

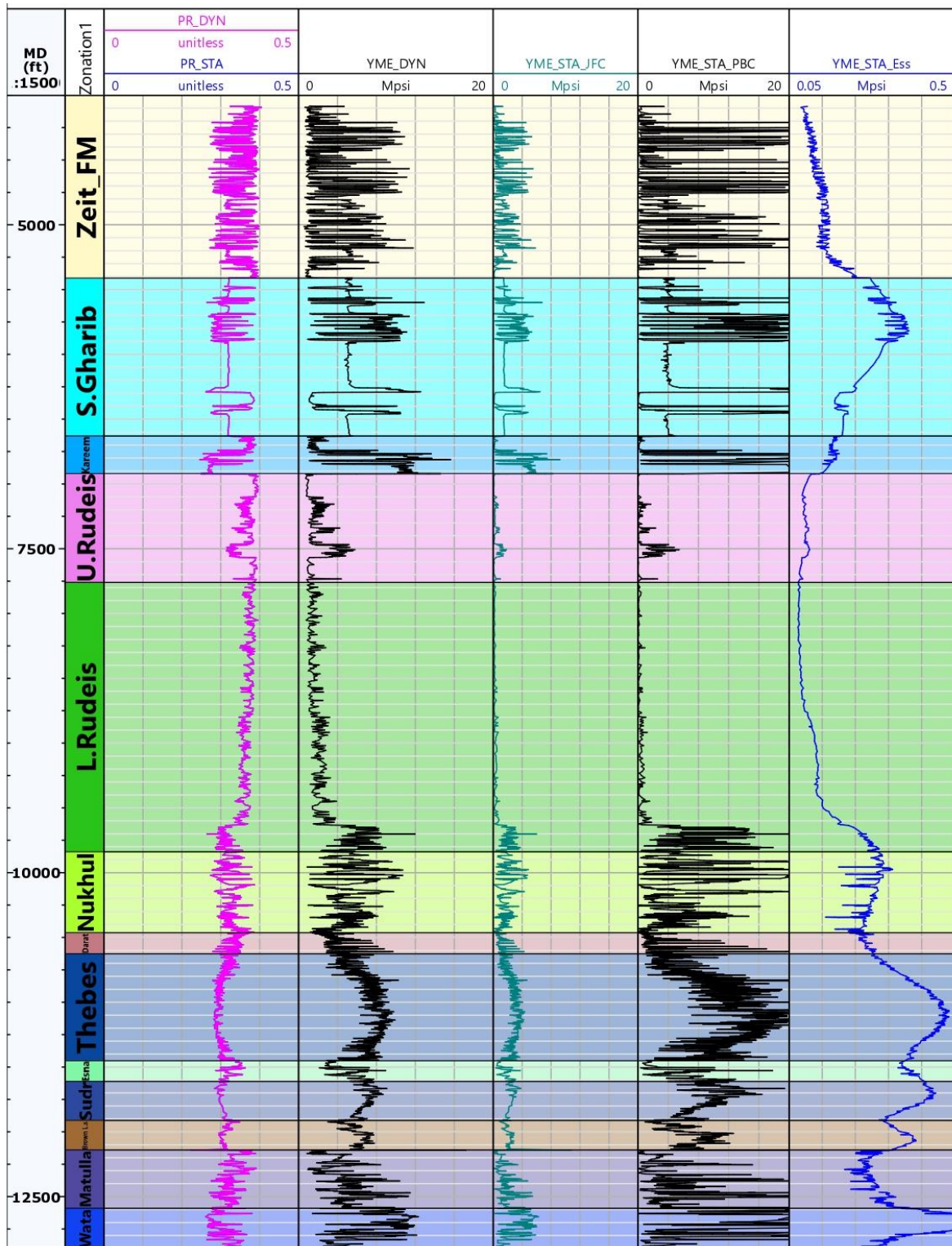


Fig. 3: the static elastic rock properties from dynamic properties calculated  $E_{dyn}$  of muzhil-7 well. **Track-1**(Depth), **track-2**(Zonation), **track-3**(PPDYN, and PP-STA), **track-4**((YM-DY), **track-5** (YMSTA-JFC), **track-6** (YMSTA-PBC), and **track-7** ((YMSTA-EISA)

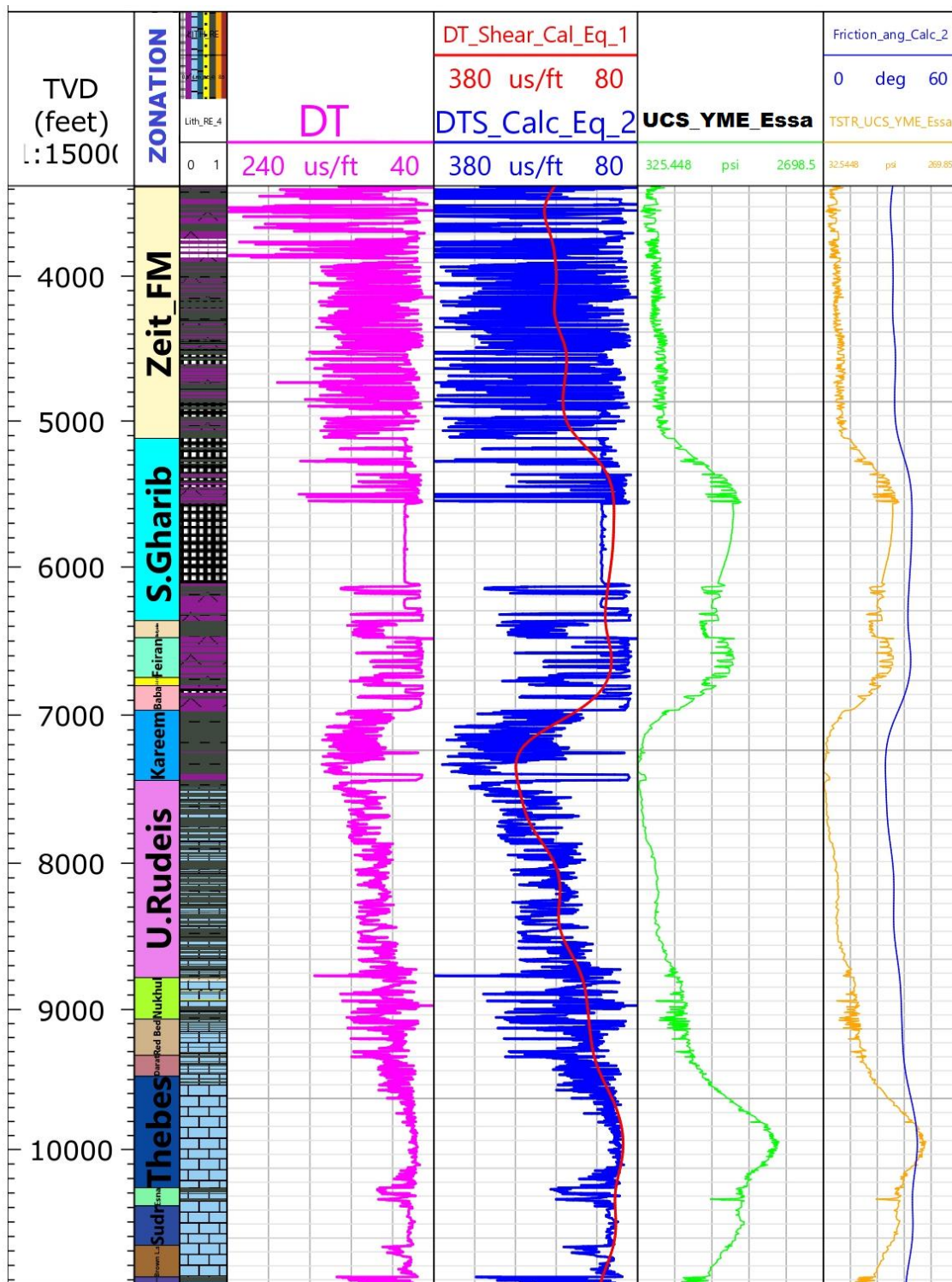
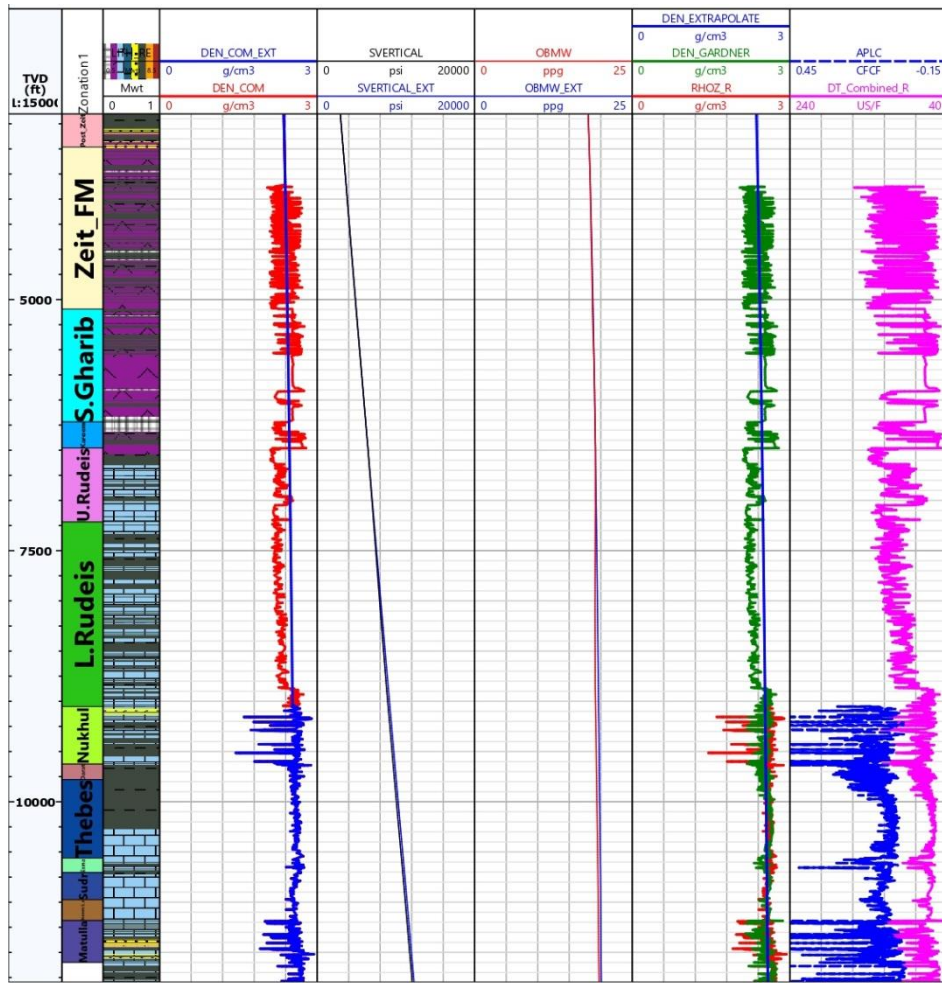


Fig. 4: The estimated UCS, friction angle, and TS for well Muzhil-7  
**Track-1**(Depth), **track-2** (Zonation), **track-3** (Lithology), **track-4** (Compressional Sonic (DT)), **track-5** (Shear Sonic calculated from EQ-1, Shear Sonic calculated from EQ-2), **track-6** (UCS), and **track-7** (friction angle, and tensile strength (TS))



**Fig. 5: Synthetic density and the output of the Sv calculation methods for Muzhil-7 well Track-1 (Depth), track-2 (Zonation), track-3 (lithology), track-4 (density combination, and density extrapolation), track-5 (Vertical stress, and Vertical stress-extrapolation), Track-6 (OBMW, and OBMW- Extrapolation), track-7 ((density- extrapolation, density Gardner, and RHOZ), and track-8 ((APLC, and DT-COM)**

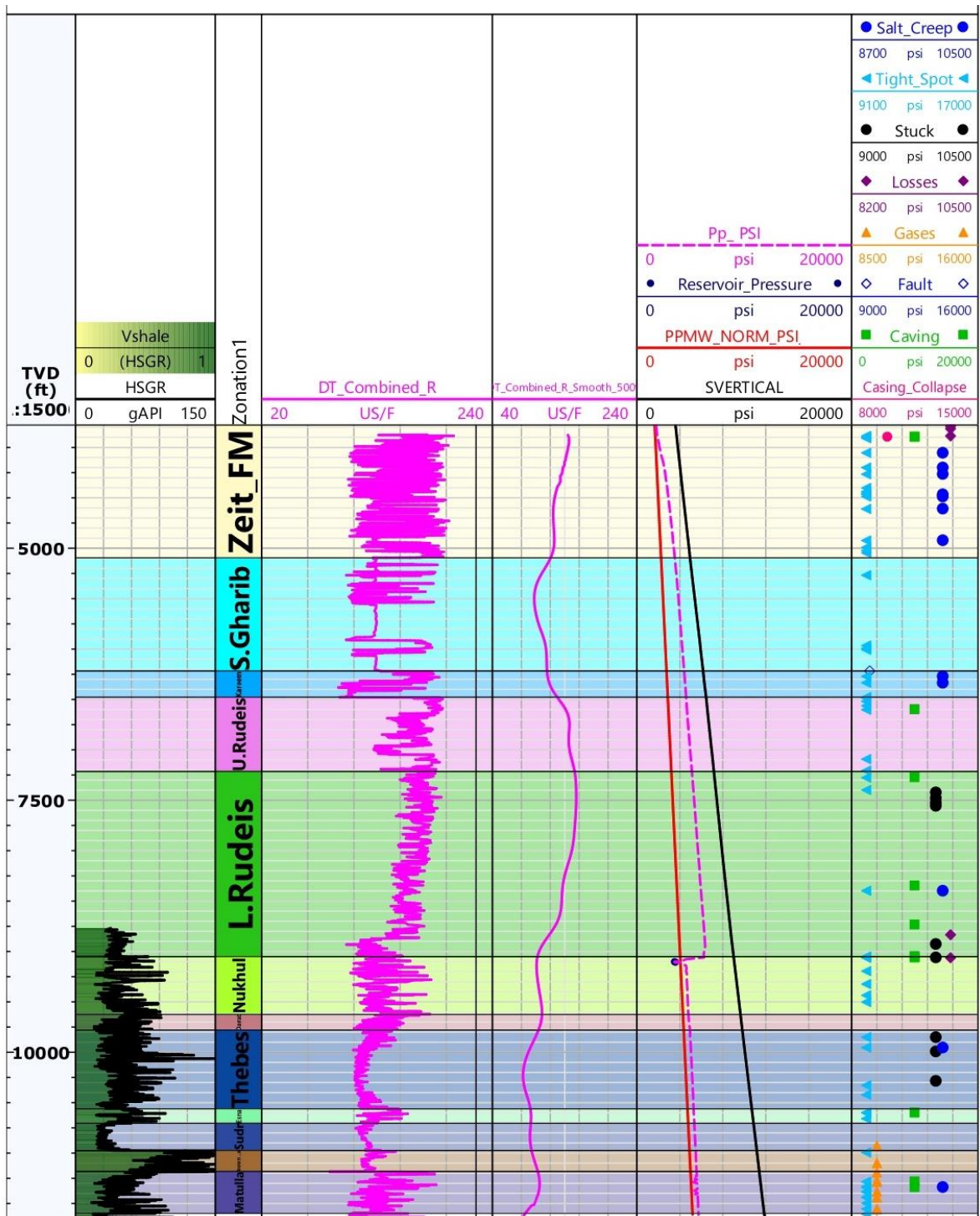
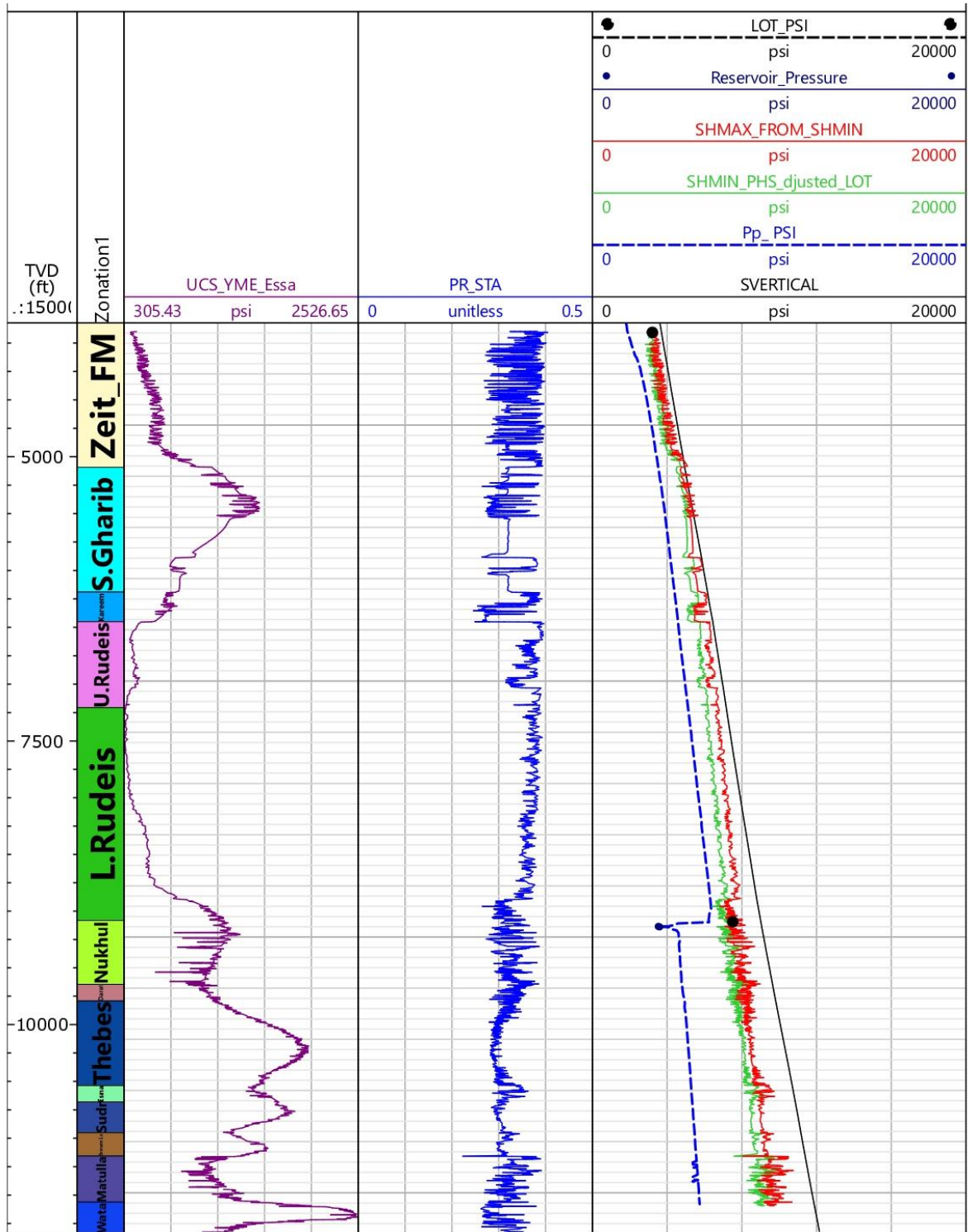


Fig. 6: Pore pressure prediction using Eaton Method

**Track 1** (Depth), **track-2** (Shale Volume), **track-3** (Zonation), **track-4** (Dt), **track-5** (DT smooth), **track-6**(Pp), reservoir pressure PPMW NORM), **track-7** (salt creep, tight spot, losses gasses, fault caving, casing collapse)



**Fig. 7: The estimated horizontal stresses magnitude for Muzhil-7 well**  
**Track-1** (Depth), **track-2** (Picks), **track-3** (UCS), **track-4** (Poisson ration), and **track-5** (LOT, reservoir pressure, SHmin, SHmax PP, and Vertical stress)

### 3. Results and discussion

Numerous calculations have been made on well logs to reveal elastic properties, rock strength, vertical and horizontal principal stresses, and Pp. These geo-mechanical factors of the Rudies Shale Formation (12.25" section) are assessed at every wellbore and integrated to build 1DMEM of the Muzhil Field.

### 3.1 Elastic Properties

Poisson's ratio( $\nu$ ) varied vertically with the stratigraphic column as revealed in Fig. 2. The estimated Static Poisson's ratio ( $\nu$  STA) were in the range of (0.30–0.39) in The Rudies Shale Formation (table 3). Therefore, it is clear that the borehole instability issues are most likely to exist in shale intervals than other zones due to the relatively high  $\nu$  and low E (0.08-0.14 Mpsi), Fig 2. Hence, the drilling MW in Rudies formations must be defined carefully.

### 3.2 Rock strength properties

The estimated friction angle (FANG) was relatively low in shale beds (27.7°–34.2°). The highest FANG values are occurred in bottom of Rudies formation (60.3°–62) and the lowest values are in the top of Rudies Formation (52°–53.7°), as presented in Fig. 4. The UCS in Rudies Shale Formation is between (300–882 psi), Fig. 4. Since TSTR is primarily calculated from the UCS (30–88.2 psi), the TSTR and UCS display the same distribution. The highest UCS and TSR values occur in bottom of Rudies formation, and the lowest values are in the top of Rudies Formation as shown in Fig. 4. There are apparent heterogeneous regions within rock strength (UCS), which plays a crucial role in WBS analysis.

### 3.3 Overburden stress and pore pressure

The 1D model of the overburden stress obviously confirms that the vertical stress( $\sigma_v$ ) rises with depth (Fig. 5). The  $\sigma_v$  of the constructed model for Rudies formation falls between 6445 and 7166 psi. Pp calculation using Eaton's method gave acceptable values for the shale unites that were reported comparable to the MDT result in the permeable intervals (13.5-13.7), fig.6. For non-shale beds, normal Pp (hydrostatic pressure) is determined using the average normal pore fluid density in Muzhil field.

### 3.4 Horizontal stress magnitude

It is detected that there are considerable variations in SHmax magnitudes (5402–6732 psi). Also, there are considerable variations in Shmin magnitudes (5025–6174 psi), fig.7. The SHmax and Shmin are observed in bottom of Rudies formation. This work focused on three common rock failure criteria namely, Mohr-Coulomb (MC), Modified Lade (ML) and Mogi Coulomb (MG) for stability analysis of four deviated wells distributed in offshore G.O.S. Also, the study describes the results of combining the MEM with MC, Mogi Coulomb and ML failure criteria to predict the wellbore breakout (WBO), mud losses, breakdown, and the effect of changing the well azimuth and inclination. The results of every formation were presented and discussed to outline the important Geo-mechanical properties, Table (2) and Fig (8).

### 3.5 Wellbore stability and safe mud weight window (MWW)

The WBS analysis of Muzhil wells is investigated to determine the safe MWW range for keeping WBS utilizing the MC, MGC, ML failure criteria. Fig. 8, Tack (7-9) shows the limits of the MWW, and the possible kick is marked near the right boundary of the grey shaded area as indicated by the MW magnitude. Instead, the minimum MW required to WBO is limited to the right limit of the yellow shaded zone. The SHmin gradient is reserved to the left boundary of the light blue area, but the formation breakdown pressure gradient is delineated by the left boundary of the dark blue zone, Fig.8. Fig. 8 shows the safe MW window of Muzhil formations using three failure criteria (MC; MGC and ML). Table (2-3) shows the ranges of the Pp, shear failure, and tensile failure boundaries. Some differences in the shear failure boundary can be seen between the results of the different failure criteria.

For a quantitative comparison of the results, Table (2-3) represents the minimum MW for the

WBS rely on three failure criteria: MC, MGC, ML. The MWWs were determined for the two-wellbore utilizing geomechanically models and failure criteria (Table 2). Consistent with the analysis, in all the boreholes, the MC breakout pressures are higher than MGC breakout pressure (Table 2). Table 2 depicts the forecast of failure criteria basic values of geomechanical parameters with their varying range. Table 3 depicts the statistical factors of principal stresses and rock mechanical parameters in Rudies shale formation in the three studied wells (rely on the 1D-MEM).

### 3.6 Sensitivity Analysis

The predominant method to evaluate the WBS sensitivity analysis to the drill path is on both stereonet plots and line plots. These plots were conducted on critical depths across the problematic formations (especially weak shale) to represent the minimum MW required to drill a borehole through the Muzhil shale Formation in any direction with any inclination. The hemisphere (stereonet) plot is a circle gridding from (0°-360°) and utilized to recognize the azimuth and inclination of the well. Well data needed to fulfil the sensitivity analysis at a single depth includes wellbore orientation, geo-mechanical model factors, and the MWW. The sensitivity analysis presents 4 diagrams. The first relation of the breakout MW with the orientation shows noticeable dark blue colour that indicates more stable wells with deviated angle between (0°- 40°). Whereas the red colour denotes the highly deviated and horizontal wellbores that showed a higher the MW value to keep the WBS, Fig.9. The second relation presents tensile failure vs. orientation and indicates that the higher limit of breakdown MW falls in N50°E orientation. Whereas the horizontal or highly deviated wells oriented to the S140°E shows the lower limit of MW as shown in Fig.9.

Fig.9a demonstrates the maximum MW that prevents formation breakdown with azimuth and deviation. Wellbores in the azimuth of SHmin have the highest breakdown MW, especially for a high-inclination or horizontal Wellbores (40°-90°). Fractures don't seem likely to take place in an inclination of (40°-90°) towards the SHmin at azimuth of N40E. Fig. 9b presents a stereo net plot that depicts the minimum MW required to prevent WBO with well azimuth and deviation. This plot suggests that the low deviation boreholes are stable in all directions. Thus, the best conditions to drill a stable borehole at this depth are to drill the wellbores in the direction of the SHmin (N40E) with a deviation of less than (40°). The plot in Fig. 9c shows the MWW with a deviation (0 –90°) and reveals that the MWW is narrowing for inclinations above 25°. Fig.9d presents the safe MWW as a function of azimuth (0–360°) and depicts that the azimuth has slight effect on the MWW at this depth and current inclination. It can be concluded that the wellbore trajectory should be designed to prevent a high deviation, or the MWWs should be high sufficient to avoid the WBO and to tolerate limited fluid loss.



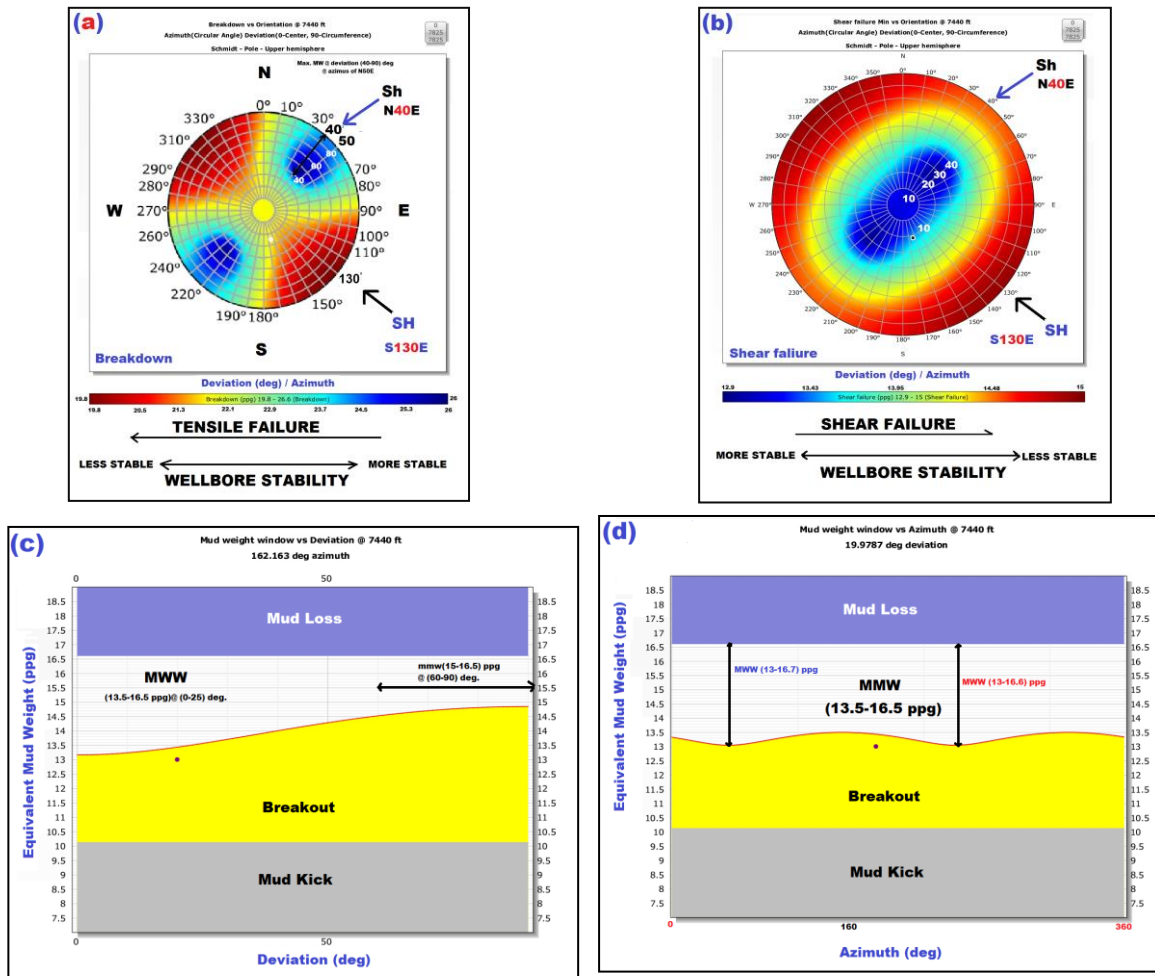


Fig. 9: Wellbore sensitivity analysis for deviation and azimuth versus breakdown and breakout MW at a single depth

(a- breakdown sensitivity to orientation, b- breakout sensitivity to orientation, c- deviation sensitivity to MW, and d- azimuth sensitivity to MW)

Table 2: minimum MW for the WBS based on three failure criteria:

| well     | Minimum mud weight (ppg) |               |              |
|----------|--------------------------|---------------|--------------|
|          | Mohr-Coulomb             | Modified Lade | Mogi-Coulomb |
| Muzhil-2 | 13.8-14.2                | 13.2-13.6     | 13-13.4      |
| Muzhil-4 | 13.7-14                  | 12.7-13.8     | 13-13.1      |
| Muzhil-7 | 14.2-14.6                | 13.7-14       | 13.8-13.9    |

**Table 3: Average values of geomechanical parameters in shale Rubies formation for all the studied wells in Muzhil Field**

| Parameters                   | Min   | Max   | Mean   |
|------------------------------|-------|-------|--------|
| Pore pressure (ppg)          | 13.5  | 13.7  | 13.6   |
| Shear failure, MC (ppg)      | 14.3  | 14.6  | 14.45  |
| Shear failure, MG (ppg)      | 13.9  | 14    | 13.95  |
| Shear failure, ML (ppg)      | 14.06 | 14.09 | 14.075 |
| MW Used(ppg)                 | 13.7  | 13.9  | 13.8   |
| Minimum MW (ppg)             | 13.8  | 14.9  | 14.35  |
| Maximum MW (ppg)             | 15.2  | 16.4  | 15.8   |
| Fracture Pressure (ppg)      | 17.2  | 17.8  | 17.5   |
| UCS (psi)                    | 380   | 882   | 631    |
| TS (psi)                     | 38    | 88.2  | 63.1   |
| Static Poisson's ratio       | 0.30  | 0.39  | 0.345  |
| Young's modulus Mpsi         | 0.08  | 0.14  | 0.11   |
| internal friction angle(deg) | 27.7  | 34.2  | 30.95  |
| SHmax magnitudes (psi).      | 5402  | 6732  | 6067   |
| Shmin magnitudes (psi).      | 5025  | 6174  | 5599.5 |

#### 4. Conclusions

One of the most significant studies in decreasing drilling activity risk and costs is the WBS evaluation in developing fields. In this study, 1D MEM was built using Techlog software 2015 for four wellbores in Muzhil field in the G.O.S. For this study, WBS was executed using 3 failure criteria. We have used datasets including well log data, drilling reports, and geological data to build a 1D MEM applicable in the study area. The results depicted many essential points that should be considered in the upcoming development of Muzhil wells in the future such as the well trajectory and MW with important impact on the WBS within the study area. The sensitivity analysis for MEM at certain depths also showed the optimal range of azimuth, deviation, and MW. In all wellbores, the failure was of breakout type and the tensile fracture type was not observed. Also, the results revealed that most of the borehole instability issues are due to insufficient MW (13 ppg). Rely on the WBS analysis results, it is recommended to increase the current MW by (0.5–1.5 ppg) to the new MW with the range of (13.5–15) to maintain the borehole wall stable during drilling operations and avoid shear failure (breakout) rely on the trajectory of the planned borehole. The results of 1-D MEM for WBS analysis shows that drilling slightly deviated and vertical boreholes parallel to the SHmin (NE40SW) with an angle of inclination less than 40° are more stable and safer than the highly deviated and horizontal wellbores. These results can be invested to reduce the high NPT and over cost of well through optimal drilling practice.

#### ACKNOWLEDGMENT

The authors wish to express their thanks and gratitude to the Egyptian General Petroleum Corporation (EGPC) and South Abu Zienima (SAZ) Company authority for permission and release of the data for this work.

## References

- [1] Liu, C., Abousleiman, Y.N., 2018. Multiporosity/multipermeability inclined-wellbore solutions with mudcake effects. *SPE J.* 23 (5), 1723–1747.
- [2] Kang, Y., et al., 2009. Wellbore stability: a critical review and introduction to DEM. In: *SPE Annual Technical Conference and Exhibition*. Society of Petroleum Engineers, New Orleans, Louisiana, p. 24.
- [3] Detournay, E., Cheng, A.H.D., 1988. Poroelastic response of a borehole in a non-hydrostatic stress field. *Int. J. Rock Mech. Min. Sci. Geomech. Abstr.* 25 (3), 171–182.
- [4] Zhang, J., Bai, M., Roegiers, J.C., 2003. Dual-porosity poroelastic analyses of wellbore stability. *Int. J. Rock Mech. Min. Sci.* 40 (4), 473–483.
- [5] Zhang, J., Roegiers, J.C., 2005. Double porosity finite element method for borehole modeling. *Rock Mech. Rock Eng.* 38 (3), 217–242.
- [6] Haimson, B., Lee, H., 2004. Borehole breakouts and compaction bands in two high-porosity sandstones. *Int. J. Rock Mech. Min. Sci.* 41 (2), 287–301.
- [7] Dresen, G., Stanchits, S., Rybacki, E., 2010. Borehole breakout evolution through acoustic emission location analysis. *Int. J. Rock Mech. Min. Sci.* 47 (3), 426–435.
- [8] Gelet, R., Loret, B., Khalili, N., 2012. Borehole stability analysis in a thermoporoelastic dual-porosity medium. *Int. J. Rock Mech. Min. Sci.* 50, 65–76.
- [9] Dokhani, V., et al., 2015. The effects of anisotropic transport coefficients on pore pressure in shale formations. *J. Energy Resour. Technol.* 137 (3).
- [10] Bradley, W.B., 1979. Failure of inclined boreholes. *J. Energy Resour. Technol.* 101 (4), 232–239.
- [11] Aadnoy, B.S., Chenevert, M.E., 1987. Stability of highly inclined boreholes (includes associated papers 18596 and 18736 ). *SPE Drill. Eng.* 2 (4), 364–374.
- [12] Roshan, H., Fahad, M., 2012. Chemo-poroelastic analysis of a borehole drilled in a naturally fractured chemically active formation. *Int. J. Rock Mech. Min. Sci.* 52, 82–91.
- [13] Rui, Z., et al., 2017. A quantitative oil and gas reservoir evaluation system for development. *J. Nat. Gas Sci. Eng.* 42, 31–39.
- [14] Yuan, J.-L., et al., 2013. Borehole stability analysis of horizontal drilling in shale gas reservoirs. *Rock Mech. Rock Eng.* 46 (5), 1157–1164.
- [15] Chen, P., Ma, T., Xia, H., 2015. A collapse pressure prediction model for horizontal shale gas wells with multiple weak planes. *Nat. Gas. Ind. B* 2 (1), 101–107.
- [16] Manshad, A.K., Jalalifar, H., Aslannejad, M., 2014. Analysis of vertical, horizontal and deviated wellbores stability by analytical and numerical methods. *J. Petrol. Expl. Prod. Tech.* 4 (4), 359–369.
- [17] Aslannejad, M., Khaksar manshad, A., Jalalifar, H., 2016. Determination of a safe mud window and analysis of wellbore stability to minimize drilling challenges and non-productive time. *J. Petrol. Expl. Prod. Tech.* 6 (3), 493–503.
- [18] Al-Ajmi, A.M., Zimmerman, R.W., 2009. A new well path optimization model for increased mechanical borehole stability. *J. Petrol. Sci. Eng.* 69 (1), 53–62.
- [19] Gholami, R., et al., 2014. Practical application of failure criteria in determining safe mud weight windows in drilling operations. *J. Rock Mech. Geotech. Eng.* 6 (1), 13–25.
- [20] S. Clark, "Handbook of Physical Constants," New York, GSA, 98-102., 1966.
- [21] Fjaer, E., Horsrud, P., Raaen, A.M., Risnes, R., Holt, R.M., 1992. *Petroleum Related Rock Mechanics*, vol. 33. Elsevier, , ISBN 9780080868912.
- [22] Allawi RH, Al-Jawad MS (2021) Wellbore instability management using geomechanical modeling and wellbore stability analysis for Zubair shale formation in Southern Iraq. *J Petrol Explor Prod Technol* 11(11):4047–4062
- [23] Allawi RH, Al-Jawad MS (2022a) 4D Finite element modeling of stress distribution in depleted reservoir of south Iraq oilfield. *J Petrol Explor Prod Technol* 12(3):679–700
- [24] Raed H. Allawi (2023) Chemical and mechanical model to analysis wellbore stability, *Petroleum Science and Technology*, DOI: 10.1080/10916466.2023.2183966
- [25] M. Zoback, "Reservoir Geomechanics (2007) " (First edition): Cambridge University Press.

- [26] Hesham Shaker Zahra a , Adel MokhlesNakhla(2015) "Deducing the subsurface geological conditions and structural framework of the NE Gulf of Suez area, using 2-D and 3-D seismic data" National Research Institute of Astronomy and Geophysics, DOI: 10.1016/j.nrjag.2015.04.003, : <https://www.researchgate.net/publication/282533743>
- [27] Eissa, E.A. and Kazi, A. (1988) Relation Between Static and Dynamic Young's Moduli of Rocks. *International Journal of Rock Mechanics and Geomechanics Abstract* 25 (6): 479-482.
- [28] Tutuncu, A.N. and Sharma, M.M., 1992, "Relating static and ultrasonic laboratory measurements to acoustic log measurements in tight gas sands," *The 67th SPE Annual Technical Conference and Exhibition*, (SPE 24689).
- [29] J. J. Zhang and R. Bentley, (2005) "Factors determining Poisson's ratio," CREWES research report, University of Calgary, Canada
- [30] N. Tutuncu, 2010 "Anisotropy, Compaction and Dispersion Characteristics of Reservoir and Seal Shales," Paper ARMA 10-344 presented at the 44th U.S. Rock Mechanics/Geomechanics Symposium and 5th U.S.-Canada Rock Mechanics Symposium, Salt Lake City,.
- [31] Chang, C., Zoback, M.D. and Khaksar, A. , 2006 "Empirical relations between rock strength and physical properties in sedimentary rocks," *Journal of Petroleum Science & Engineering*, 51, 223-237.
- [32] M. Lal (1999) "Shale Stability: Drilling Fluid Interaction and Shale Strength. .," SPE 54356, SPE Latin American and Caribbean Petroleum Engineering Conference held in Caracas, Venezuela.
- [33] Scott, D.R., Thomsen, L.A., 1992. U.S. Patent No. 5,081,612. U.S. Patent and Trademark Office, Washington, DC. Sen, S., Kundan, A., Kalpande,
- [34] Eaton, B.A., 1975. The equation for geopressure prediction from well logs. Fall meeting of the Society of Petroleum Engineers of AIME, Dallas, Texas
- [35] Zhang J (2011) Pore pressure prediction from well logs: methods, modifications, and new approaches. *Earth Sci Rev* 108(1):50–63
- [36] Moos, D.; Zoback, M.D. 1990 Utilization of observations of well bore failure to constrain the orientation and magnitude of crustal stresses: Application to continental, Deep Sea Drilling Project, and Ocean Drilling Program boreholes. *J. Geophys. Res. Solid Earth* 1990, 95, 9305–9325.
- [37] A. Al-Ajmi, " Wellbore stability analysis based on a new true-triaxial failure criterion.," Doctor of Philosophy thesis, land and water resources engineering department, KTH Royal Institute of Technology., Sweden, 2006.
- [38] M. Zoback, "Reservoir Geomechanics," (First edition): Cambridge University Press, 2007.
- [39] K. Mogi, "Fracture and Flow under High Triaxial Compression.," *Journal of Geophysical Research*. Res. 76: 1255–1269., 1971.
- [40] A. Al-Ajmi, "Mechanical Stability of Horizontal Wellbore Implementing Mogi-Coulomb Law.," *Advances in Petroleum Exploration and Development*, 4(2), 1–8. <https://doi.org/10.3968/j.aped.1925543820120402.843>, 2012.
- [41] A. Al-Ajmi, "Mechanical Stability of Horizontal Wellbore Implementing Mogi-Coulomb Law.," *Advances in Petroleum Exploration and Development*, 4(2), 1–8. <https://doi.org/10.3968/j.aped.1925543820120402.843>, 2012.
- [42] P. Lade, "Elasto-plastic stress-strain theory for cohesionless soil with curved yield surfaces," *International journal of solids and structures*, 13(11), 1019-1035., 1977.
- [43] A R. Ewy, "Wellbore-stability predictions by use of a Modified Lade criterion," *SPE Drilling & Completion*. (SPE-56862). Res. 14: 85–91, 1999.
- [44] R. Rahimi, "The effect of using different rock failure criteria in wellbore stability analysis," Master of Science theses, Geosciences and Geological and Petroleum Engineering, Missouri University and Technology. Retrieved from <http://mst.bepre>, 2014.



## APPENDIX

### Mohr Coulomb (MC) failure criterion

The MC failure criterion is the simplest and most widely used criterion for WBS analysis. It is relied on the pioneer extensive experimental investigations done by Coulomb, 1773[37]. This criterion is a type of 2D failure criterion and assumes which the intermediate principal stress has not any impact on the failure. Based on the tri-axial strength experiment, Fig. 10(B), Mohr found that the shear stress required to fail the rock must overcome the friction resistance between particles and the cohesive strength ( $c$ ) that bond the rock grains together [37-38].

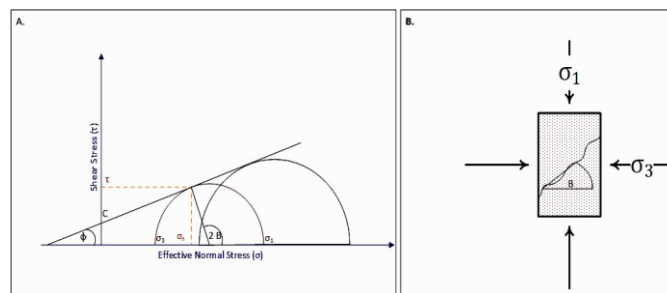


Fig.10: (A) Mohr-Coulomb failure criterion, (B) shear failure of a rock sample or triaxial strength test

According to the MC failure criterion, the require shear stress for failure increases with increasing the confined stress ( $\sigma_3$ ), as represented by straight line of Fig. 10 (A), consequently the shear stress  $\tau$  equals to Equation 14.

$$\tau = c + \sigma \tan \phi \quad (14)$$

Where ( $c$ ) is the cohesion that resists the particle movement, it represents the shear stress at zero normal stress. ( $\phi$ ) is the angle of internal friction which is the angle between the tangential of Mohr's circles and horizontal line. ( $\sigma$ ) is the effective normal stress. The coefficient of internal friction is commonly used which equals to the slope of the tangential line, Equation 15.

$$\mu = \tan \phi \quad (15)$$

The sample fracture angle ( $B$ ) related to the angle of the internal friction  $\phi$  by Equation 16.

$$B = 45^\circ + \frac{\phi}{2} \quad (16)$$

The Mohr-Coulomb criterion could be presented regarding to the principal stresses by Equation 17.

$$\sigma_1 = c_o + \sigma_3 q \quad (17)$$

Where ( $c_o$ ) is the uniaxial compressive strength (UCS) which is  $\sigma_1$  when  $\sigma_3 = 0$  i.e., no confining pressure.  $c_o$  is related to the rock cohesion, and angle of internal friction, Equation 18. The factor ( $q$ ) is function of the internal angle of friction Equation 19.

$$c_o = 2c \frac{\cos \phi}{1 - \sin \phi} \tag{18}$$

$$q = \frac{1 + \sin \phi}{1 - \sin \phi} \tag{19}$$

The Mohr-Coulomb failure criterion gives a good result when  $\sigma_2 = \sigma_3$ , which equivalent to the result from the 3D failure criteria. However, the Mohr-Coulomb failure criterion underestimates the formation strength that can result in overestimation of the require mud weight to drill the well.

**Mogi-Coulomb failure criterion**

The polyaxially compressive tests were carried out for the first time by Mogi [39]. He found that, there is an important impact of the intermediate principal stress on rock strength and rock failure [40]. The brittle fracture arises along a plane that strikes in the direction of the intermediate principal stress [37]. Based on a set of triaxial test, Mogi found that the fracture plan creation is a function of mean effective stress ( $\sigma_{m,2}$ ) instead of the octahedral normal stress ( $\sigma_{oct}$ ), this explains why the fracture plane is initiated in the direction of ( $\sigma_2$ ). Consequently, Mogi observations led to introduce a rock failure criterion that considers the intermediate principal stress effect. He assumed that there is a linear proportional relationship between distortional strain energies and octahedral shear stresses ( $\tau_{oct}$ ). This linear relationship will continue until failure threshold is exceeded. Al-Ajmi and Zimmerman [37] found the best linear fit of the triaxial data as in Fig. 11.

$$\tau_{oct} = a + b\sigma_{m,2} \tag{20}$$

Where ( $a$ ) and ( $b$ ) are Mogi strength parameters, ( $a$ ) is the intercept of the line and ( $b$ ) is the slop of the line. ( $\tau_{oct}$ ), and ( $\sigma_{m,2}$ ) can be evaluated from Equation 22.

$$\tau_{oct} = \frac{1}{3} \left( \sqrt{(\sigma_1 - \sigma_2)^2 + (\sigma_2 - \sigma_3)^2 + (\sigma_3 - \sigma_1)^2} \right) \tag{21}$$

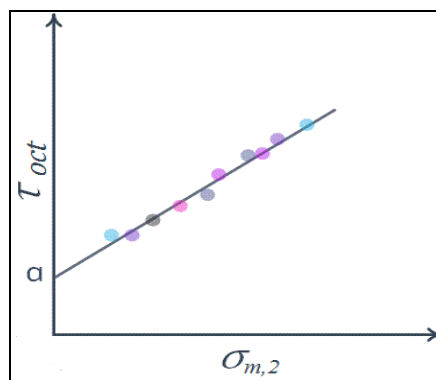


**Fig. 11: Mogi-Coulomb failure criterion for triaxial test data**

$$\sigma_{m,2} = \frac{\sigma_1 + \sigma_3}{2} \tag{22}$$

The Mogi-Coulomb failure criterion is considered one of the most accurate criteria for sedimentary rocks like shale.it reduced to Mohr-Coulomb failure criterion when  $\sigma_2 = \sigma_3$ . Al-Ajmi and

Zimmerman [37] [41] proposed equations for obtaining the parameters ( $a$ ) and ( $b$ ) from similar Mohr-Coulomb parameters ( $q$ ) and ( $c_o$ ), where parameter ( $b$ ) is corresponding to the internal friction, Equation 23, while the parameter ( $a$ ) is corresponding to internal friction and cohesion, Equation 24.

$$a = \frac{2\sqrt{2} c_o}{3 q+1} \quad (23)$$

$$b = \frac{2\sqrt{2} q-1}{3 q+1} \quad (24)$$

**Modified Lade Failure Criterion.**

In 1977, Lade conducted many experiments on cohesionless soil, like granular soil. He found that there is inverse relationship between the frictional angle and the mean normal stress [42]. The Lade criterion is given by Equation 25.

$$\left(\frac{I_1^3}{I_3} - 27\right) \left(\frac{I_1}{P_a}\right)^{m'} = \eta_1 \quad (25)$$

Where  $I_1$  and  $I_3$  are the first and third invariants of the stress tensor,  $P_a$  is the atmospheric pressure,  $m'$  and  $\eta_1$  are the material constant. In 1999, Ewy introduced the ML criterion [50]. He assumed that  $m'$  that makes the original Lade criterion be able to predict the linear shear strength increase with increasing the mean normal invariant stress ( $I_{1/3}$ ). The original Lade criterion is introduced for cohesionless material however to consider the material with cohesion, Ewy [43] introduced a new parameter ( $S$ ) which is function in the rock cohesion and ( $\eta$ ) which related to the internal friction. The ML criterion is given by Equation 26.

$$\frac{I_1'^3}{I_3'} = 27 + \eta \quad (26)$$

where:

$$I_1' = (\sigma_1 + S) + (\sigma_2 + S) + (\sigma_3 + S) \quad (27)$$

$$I_3' = (\sigma_1 + S)(\sigma_2 + S)(\sigma_3 + S) \quad (28)$$

The advantages of ML criterion are that it considers the intermediate principal stress impact and Lade parameters can be obtained from tri-axial tests similar to MC parameters cohesion and FANG [44]. This makes this criterion easy to use, and potentially more descriptive for rock failure when considering problems such as WBS [38].

$$S = \frac{c}{\tan \phi} \quad (29)$$

$$\eta = \frac{4 \tan \phi^2 (9 - 7 \sin \phi)}{(1 - \sin \phi)} \quad (30)$$

Where ( $C$ ) is the rock cohesion, it can be calculated using Equation 18. The accuracy of ML criterion sharply decreases in tensile stress incidence. However, this doesn't have any effect on the accuracy of WBS analysis because the analysis focuses on finding the required MW to avoid shear failure [43-44].

## إدارة مخاطر عدم استقرار جوف البئر باستخدام النمذجة الجيوميكانيكية وتحليل استقرار جوف الآبار لتكوين مزل في الطفلى فى خلىج السوىس ، مصر

### الملخص

يشكل عدم استقرار جوف البئر مخاطر محتملة أثناء عملية حفر الآبار ؛ قد تسبب هذه المخاطر حالات معقدة ، وفي بعض الحالات ، يمكن أن تسبب هذه المشاكل حالات معقدة ويمكن أن تؤدي في بعض الحالات إلى مشكلات تشغيلية مكلفة. في هذه الدراسة نقدم أفضل الحلول من خلال التنبؤ والقياس الكمي لعدم استقرار جوف البئر في حقل مزل ، خليج السويس ، باستخدام نموذج أرضي ميكانيكي أحادي البعد (D-MEM<sup>1</sup>) تم بناؤه اعتماداً على سجلات الآبار وقياسات الضغط وتقارير ظروف الحفر. أنشأنا أولاً النموذج الأرضي الميكانيكي أحادي البعد (1D-MEM) عن طريق حساب ضغط المسام ، والضغط العمودي ، وقوة الصخور ، ومعايير مرونة الصخور ، والضغوط الأفقية. وقد حددت معايير الانهيار (معياري موهر كولمب ومعياري لاد المعدل ومعياري موجي كولمب) إمكانية تشوه البئر. أخيراً ، أمكن استخدام نموذج الأرض الميكانيكي أحادي الأبعاد (D-1 MEM) لإجراء تحليل شامل لاستقرار جوف البئر الجيوميكانيكي لمناطق المشاكل في تكوين مزل قيد الدراسة. أظهرت نتائج نموذج الأرض الميكانيكي أحادي الأبعاد (D-MEM<sup>1</sup>) أن أفضل سمت (azimuth) للآبار الرأسية والمائلة ميلاً خفيفاً ستكون (٤٠ - ٦٠ درجة) في اتجاه عقارب الساعة من الشمال ، أي موازية لـ SHmin أى (NE40SW) . أظهر تحليل ثبات حفرة البئر أن جوف البئر العمودية والمنخفضة الميل (أقل من ٤٠ درجة) آمنة وأكثر ثباتاً من جوف البئر الأفقية والمرتفعة الميل وأن وزن الطين (MW) غير المناسب هو سبب رئيسي لعدم استقرار جوف البئر. الحل الأمثل لعدم استقرار جوف البئر هو اتباع مسار البئر الأمثل واستخدام وزن طين آمن . يتراوح الوزن الأمثل للطين في تكوين الطفلة من ١٣,٥ - ١٥ ppg. تساهم نتائج البحث في خطة تطوير الآبار القريبة من منطقة الدراسة وتقليل الوقت والتكلفة غير المنتجين.